Volume 0 (1981), Number 0 pp. 1–15 COMPUTER GRAPHICS *forum*

Allometric Scaling for Character Design

T. McGraw, T. Kawai and J. Richards

West Virginia University & Morgantown, WV, USA

Abstract

Geometric scaling transformations do not respect the biological processes which govern the size and shape of living creatures. In this paper we describe an approach to scaling which can be related to biological function. We use known biological laws of allometry which are expressed as power laws to control the mesh deformation in the frequency domain. This approach is motivated by the relation between fractal biological systems and their underlying power-law spectra. We demonstrate our approach to biology-aware character scaling on triangle meshes representing quadrupedal mammals.

Categories and Subject Descriptors (according to ACM CCS): I.3.3 [Computer Graphics]: Picture/Image Generation—Line and curve generation

1. Introduction

The design of virtual living characters for movies, games and other computer graphics applications is largely an artistic endeavor. As a result, biological issues are often overlooked during character design. By incorporating known relations between scale and biological function into the character design process we can force the resulting data to be biologically plausible. This simplifies the process of character design, permitting the designer to manipulate the geometric form of a character by setting a few scale parameters, and to generate a spectrum of characters at different scales from a single mesh. This process can also provide insight into the relations between form and function of living creatures by allowing the user to explore the space of plausible creatures. In this paper we present a method of incorporating known correspondences between biological function and geometric form in the character editing process using spectral mesh processing techniques.

Characters are typically modeled as triangle meshes consisting of thousands or more vertices. Editing these triangle meshes can be time consuming due to the large number of vertices. The number of variables needed to specify a mesh can be reduced by using modeling techniques such as splines or subdivision surfaces. Another approach, spectral mesh processing, allows us to represent the mesh as a combination of manifold harmonic basis functions. This permits meshes with hundreds of thousands of vertices to be manipulated in terms of about a thousand variables, and simplifies many processes such as mesh filtering, segmentation, and computation of the mesh skeleton. We further reduce the number of variables to fewer than 10 by finding the combinations of coefficients with anatomical and biological meaning.

In this work we simplify the character design process by incorporating known empirical relations between biological function and geometrical measurements. These relations are used to constrain the editing in terms of manifold harmonic coefficients. In this work we consider constraints which involve the cardiopulmonary system, the metabolic system, and biomechanical stresses due to locomotion.

Character modeling using such biological relations will simplify editing of meshes representing living creatures. This can lead to more efficient generation of biologically plausible character designs.

2. Background

The study of the connection between form and function is an old one. One of the earliest to discuss the topic was Galileo [GCFdS54] who was especially interested in how changes in scale affected the shape of certain mechanisms and animals. This line of questioning was also pursued in the early 1900s by Haldane [Hal28], later by Thompson [Tho52], and more recently by Bonner [Bon69, Bon06]. The relations between biological function and anatomical form can be expressed as

© 2010 The Author(s)
Journal compilation © 2010 The Eurographics Association and Blackwell Publishing Ltd.
Published by Blackwell Publishing, 9600 Garsington Road, Oxford OX4 2DQ, UK and 350 Main Street, Malden, MA 02148, USA.

Figure 1: *1950s Sci-Fi and Horror movies featured many characters scaled to fantastic degrees. The isometric scaling performed to create these characters is implausible for physical and biological reasons.*

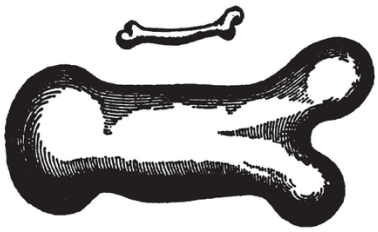

Figure 2: *Galileo's sketch of two bones. One is three times as long as the other, but the larger bone must have a different shape if it is to perform the same function as the smaller bone.*

mathematical models which are theoretical in nature, or they can be based on observations and measurements of many species (such as the allometric laws discussed later).

The "square-cube law" refers to the relation between volume and cross-sectional area as objects undergo dramatic scaling, and it can have biomechanical consequences. These consequences are often described in the context of the extreme scaling transformations depicted in 1950's horror movies such as "Attack of the 50 Foot Woman" or "Them", which features giant mutated ants. These fantastic characters, shown in Figure (1), are unrealistic due to changes in proportionality between volume and area that are required when objects undergo scaling transformations. The square-cube law states that applying a uniform scaling factor, s, to each dimension of an object causes the volume to increase by a factor of s^3, but the cross-sectional area only increases by a factor of s^2. Assuming that material properties are unchanged by the scaling, the weight of the object will scale by s^3, but the structural ability of the object to resist tensile and shear stresses will only scale by s^2. What this means for the 50 foot woman is that she would collapse under her own weight. Our method of character design permits artists to easily generate plausible character designs with respect to such scaling.

2.1. Historical Perspective

Galileo published many observations regarding the scale of mechanisms and structures [GCFdS54], including a discussion of the scale of living creatures. This was accompanied by the sketch in Figure (2) which shows the changing proportions of a bone which scales to 3 times its original length. He observed that the bone does not simply scale uniformly - it must change shape. Specifically, the larger bone must be thicker in order to support the increased weight it must bear. This can be seen as a biological example of the design principle "form follows function." Galileo admits that changes in material may mitigate the effects of scale, as will buoyancy as demonstrated by large fish and whales whose skeleton cannot support their weight outside of the water. In this work we concentrate on terrestrial animals to avoid such concerns.

Haldane [Hal28] also described the relation between structure and scale in his essay "On Being the Right Size", though he did not explicitly reference Galileo's work. *Haldane's principle* states that the structure and complexity of living organisms is dictated by their size as well as function. He gives examples of possible changes in structure which may compensate for changes in scale

> "...suppose that a gazelle, a graceful little creature with long thin legs, is to become large, it will break its bones unless it does one of two things. It may make its legs short and thick, like the rhinoceros, so that every pound of weight has still about the same area of bone to support it. Or it can compress its body and stretch out its legs obliquely to gain stability, like the giraffe."

These are exactly the types of transformations of shape we propose to model in response to changes in scale.

2.2. Allometric laws in biology and other sciences

"Allometric change" or "differential scaling" occurs when the proportions of an organism adjust in response to changes in size or other parameters. The term "allometry" was coined by Julian Huxley [Hux32] who presented the first allometric laws relating body weight to quantitative biological properties.

Allometric laws relate 2 biological characteristics, and commonly take the form of a power law, $X = aY^b$. Laws of this form may be linearized by taking the logarithm of both sides, $\log X = \log a + b \log Y$. For example Kleiber's law, $B = aM^{3/4}$, relates metabolic rate, B, and body mass, M.

© 2010 The Author(s)
Journal compilation © 2010 The Eurographics Association and Blackwell Publishing Ltd.

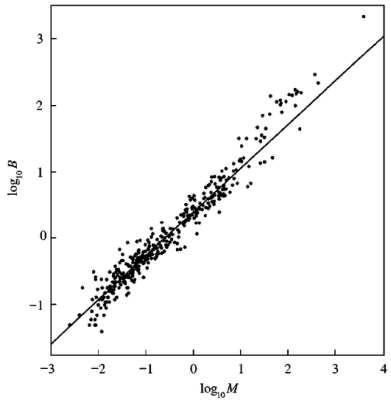

Figure 3: *Allometric relation between metabolism and mass for 391 species of mammal. The relation is linear when plotted on a log-log scale. Figure from Dodds et al. [DRW01]*

Although many of these laws are based on empirical observations they often hold true over a large number of species. A log-log plot of Kleiber's law over 391 species is shown in Figure (3). Allometric laws can be roughly classified in terms of the value of the exponent, b. If $b = 1$ the relation is linear, and the mass scaling is a linear function of the biological variable (isometric scaling). If $b < 1$ the relation is a 'negative allometry', and X increases relatively slowly as Y increases. The case of $b > 1$, 'positive allometry' implies that X increases quickly relative to Y. If $b = 0$ then X is invariant with respect to Y. A familiar example of negative allometry is the relation between head size and body mass. Juvenile animals typically have large heads relative to their body weight. As they age the body weight increases more quickly than the head size, so that in the adult the head is proportionally smaller relative to the body.

The influential biologist Stephen J. Gould [Gou66] suggested that allometry was more than the mere study of such power laws, but that it was "the study of size and its consequences." Because many of these laws are expressed in terms of mass, length or area, they are useful in developing plausible scaling transformations. Allometric laws involving many physiological systems have been proposed, including circulatory [Li96] and cardiovascular models [Tor98]. As a statistical tool, allometry has proven to be useful for comparative physiology.

West [WBE97] established a connection between allometric laws and the fractal structure of biological systems, such as the branching networks of tubes forming vascular and respiratory systems. In fact, allometric relations often arise in the study of non-biological systems with self-similar or self-affine structure at many scales. Kolmogorov's $5/3$ law governs turbulence at multiple scales in fluids and can be exploited in fluid simulation and animation [SF93, Bri08]. The law was derived by Kolmogorov from theoretical principles, not empirical observations, and relates the energy contained in each wavenumber (or spatial frequency) to the wavenumber itself through the power law $E(k) = Ck^{5/3}$. The connection between natural systems exhibiting fractal geometry and power laws in the spectral domain shows up in many other areas.

Mandelbrot and Van Ness [MVN68] first established that self-affine processes have a power spectrum in the form of a power law. Furthermore, the power law exponent is directly related to fractal dimension. One particular process, fractional Brownian motion has been used in computer graphics to generate fractional Brownian surfaces which are useful as terrain models [Man79]. Power-law filtering of Fourier coefficients is used in studies of geology [LDC93], to describe rain and clouds [SL87], and in analyzing images of sea ice [FFL*96].

'Pink noise' or '1/f noise' with a spectral density $S(f) = C/f^{\alpha}$ occurs in many natural phenomena. Some approaches to procedural texture generation are based on controlling image spectra to impose the '1/f' structure [Ebe03]. A well-known example is the *turbulence* function described by Perlin [Per85]. In fact, the power spectrum of natural images is known to obey a power law relation [RSAT04].

In this paper we explore the extension of these concepts to mesh processing. The manifold harmonic transform provides us with a frequency domain representation of the mesh, and a means of directly manipulating the power spectrum. We observe that the power spectrum of character meshes obeys a power law, just as natural images do. We will show that power-law filtering of the mesh spectrum results in allometric scaling of the mesh. Then, using known biological allometric relations we can control local scaling to generate biologically plausible changes in shape.

2.3. Biological Approaches to Graphics

Models of biological processes have been exploited to improve the realism of graphics applications. Previous examples of biologically inspired graphics include the 'artificial life' proposed by Terzopoulos [Ter99, Ter08]. Much work in this area has concentrated on modeling of behaviors, such as flocking and herding of groups [Rey88].

Lee [LST09] used biomechanical modeling for simulation and animation. Tu [Tu99] developed models based on the biomechanics and locomotion of fish. Terzopoulos [TW90] utilized biomechanical models of the head for facial animation. Ijiri et al. [IYKI08] developed a system for realistic animation of opening flowers. The reaction-diffusion process proposed by Turing [Tur52] as an explanation for patterns on animal skins has been used to generate texture maps with an organic appearance [WK91, Tur91].

Unlike this previous work, we do not propose to generate any animation or to numerically simulate any process.

© 2010 The Author(s)
Journal compilation © 2010 The Eurographics Association and Blackwell Publishing Ltd.

Instead our goal is to model how biological processes influence changes in shape. Along those lines, there have been several other approaches taken for structural generation of plants [Pru86, PL90, PHL*09]. Unlike this work, we do not generate a mesh, we modify an existing mesh.

Several previous works have utilized numerous range-scans to learn the parameterization of shape-space. The space of human body shapes was parameterized by Allen et al. [ACP03] and they demonstrated a method to generate realistic meshes with anatomical features of varying size and shape. Anguelov et al. [ASK*05] presented a human body animation model which incorporated changes in shape and pose. They used principal components analysis to find a low-dimensional space of parameters which described variation in shape, but also required numerous range scan data as input. Unlike these methods, our method requires only a single input mesh and exploits known measurements and relations which abound in the biology and morphometry literature.

2.4. Spectral Mesh Processing

The manifold harmonic transform which we use for processing character meshes is a product of the active research area of spectral mesh processing. Spectral methods, in general, involve analysis of the eigenvalues and eigenvectors of appropriately defined matrices. These methods have been applied to many topics in the visualization, graphics and pattern recognition fields.

Liu and Zhang [LZ04] applied spectral clustering to 3D **mesh segmentation**. The selected eigenvectors of the affinity matrix or the closely related graph Laplacian were used. Katz et al. [KLT05] presented an algorithm for segmenting a mesh into visually meaningful sub-meshes. Zhang and Liu [ZL05] described a mesh segmentation algorithm based on recursive spectral 2-way cut and Nyström approximation. De Goes et al. [dGGV08] presented a segmentation method to assist the rigging of articulated bodies. We will make use of spectral mesh segmentation to restrict scaling and other shape changes to the relevant anatomical areas.

Vallet and Lévy [VL08] presented a method to convert the geometry of a mesh into frequency space for the purposes of **mesh smoothing**. The eigenfunctions of the Laplace-Beltrami operator are used to define Fourier-like basis functions called manifold harmonics. High frequency noise and other details can be removed by low-pass filtering. The manifold harmonics are described in further detail in the next section.

Spectral methods have also led to new methods of **mesh parameterization**. Gotsman et al. [GGS03] discussed parameterizing a triangle mesh onto the sphere, and also a generalization of the method of barycentric coordinates for planar parameterization. Zhou et al. [ZSGS04] presented a fully automatic method, called iso-charts, for creating texture atlases on arbitrary meshes. Mullan et al. [MTAD08] presented a spectral approach to automatically obtain discrete free-boundary conformal parameterization of triangle mesh patches. Zigelman et al. [ZKK02] presented a technique for **texture mapping** on arbitrary surfaces with minimal distortions by preserving the local and global structure of the texture.

Other applications of spectral methods include **symmetry detection** [OSG08], **surface reconstruction** [KSO04], **remeshing** [DBG*06], **mesh compression** [BCG05, ZB04, Zha04] and **shape correspondence** [MCBH07,JZ07,LH05]. See Zhang et al. [ZvKD07] for a more complete survey.

2.4.1. Manifold Harmonics

The manifold harmonic basis (MHB) is analogous to the sinusoidal basis implied by the Fourier transform - both are eigenfunctions of Laplacian operators defined on their respective spaces. The Fourier transform operates on functions of real variables, but the manifold harmonic transform (MHT) operates on functions whose domain is a discrete graph representing the connectivity of the mesh.

Given a triangulated mesh with n vertices we may compute m basis functions $H^k, k = 1...m$ called the manifold harmonic basis. Each basis function is assumed to be a piecewise linear function represented by its value H_i^k at each vertex, i. These basis functions, in matrix form, can be used to transform the vertices back and forth between their native geometric space and the frequency domain. Let $x = [x_1, x_2, ...x_n]$, $y = [y_1, y_2, ...y_n]$, and $z = [z_1, z_2, ...z_n]$ be the geometric coordinates and $\tilde{x} = [\tilde{x}_1, \tilde{x}_2, ...\tilde{x}_m]$, $\tilde{y} = [\tilde{y}_1, \tilde{y}_2, ...\tilde{y}_m]$, $\tilde{z} = [\tilde{z}_1, \tilde{z}_2, ...\tilde{z}_m]$ be the frequency coordinates.

The frequency domain vertices can be computed using the manifold harmonic transform

$$\tilde{x} = xDH, \tag{1}$$

where D is a lumped mass matrix which depends on triangle areas within the mesh. Similar expressions hold for $\tilde{y}, \tilde{z}$.

The mesh may be reconstructed from the frequency domain vertices by

$$x = \tilde{x}H', \tag{2}$$

where H' is the transpose of H. Similar expressions can be written for y, z.

Spatial frequencies, ω_i, of the basis functions are related to the eigenvalues, λ_i, associated with each eigenvector by $\omega_i = \sqrt{\lambda_i}$. A frequency-space filter can be implemented by multiplying the frequency coordinates with filter weights, f during reconstruction

$$x = \tilde{x}FH', \tag{3}$$

where F is a diagonal matrix whose entries are given by f. The filtering achieved by this process is similar to filtering time domain signals using the Fourier transform : low pass filtering can be implemented by attenuating the coefficients

© 2010 The Author(s)
Journal compilation © 2010 The Eurographics Association and Blackwell Publishing Ltd.

Mesh	Vertices	α	R
Horse	19851	-1.39	-0.927
Camel	21887	-1.17	-0.900
Hippo	22264	-1.24	-0.832
Cow	2903	-1.14	-0.864
Elephant	3752	-1.21	-0.903
Pig	3522	-1.23	-0.894
Giraffe	9239	-1.27	-0.879
Cat	7207	-1.35	-0.906

Table 1: *Correlation coefficients between* $\log\tilde{r}$ *and* $\log\lambda$. *Values of R closer to* -1 *imply a linear relationship between these variables, and therefore that the mesh spectrum obeys a power law.*

of high frequency basis functions. Details may be enhanced by boosting the same coefficients. When filter coefficients are all equal, $f = [a, a, ..., a]$ the filter performs an isometric scaling by factor a.

We perform allometric mesh scaling in terms of these filter coefficients by giving anatomical and functional meaning to certain combinations of coefficients. Usually, directly manipulating filter coefficients is not an intuitive way to edit a mesh. In general terms f_i controls low-frequency shape when λ_i is low, and high frequency detail when λ_i is high, but it is difficult to achieve desirable results when manually changing these coefficients. Mesh editing in terms of these filter coefficients has potential to be a powerful tool if they can be controlled in a meaningful way. For example, Rong et al. [RCG08] performed mesh deformation in terms of manifold harmonics, but the deformations described were changes in pose, not shape. Our work will connect biological and physiological function to mesh shape through these filter coefficients.

3. Implementation

We implemented the manifold harmonic decomposition as described by Vallet and Lévy [VL08] and applied it to mesh data from public mesh repositories. Results for a horse mesh are shown in this section.

A plot of the absolute value of manifold harmonic coefficients for the horse mesh is shown in Figure (4). The coefficients roughly obey a power law with respect to eigenvalue, and therefore also frequency. We observe this behavior over all of our input meshes and note the similarity to natural images which are also characterized by power law spectra. For 2-dimensional natural images the spatial frequency domain is also 2-dimensional. The spectrum for images is commonly determined by circular averaging to obtain a 1-dimensional radial spectrum [RSAT04]. We similarly represent the spectrum of meshes in terms of the radial spectrum $\tilde{r} = \sqrt{\tilde{x}^2 + \tilde{y}^2 + \tilde{z}^2}$.

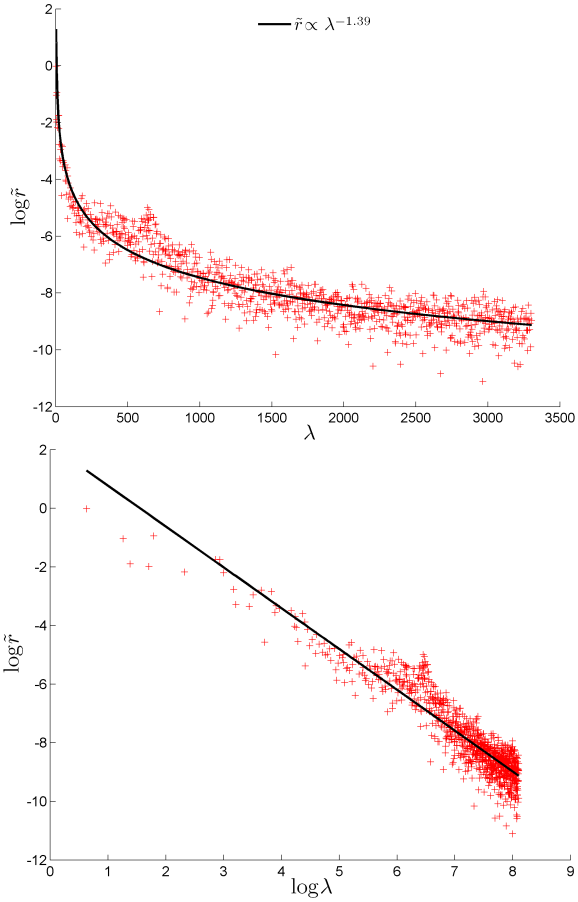

Figure 4: *Manifold harmonic coefficients plotted on a semilog scale (top) and log-log scale (bottom). Red crosses are* $\tilde{r}$ *radial spectrum coefficients. The solid lines shown for reference are the approximate power law curve computed by linear regression in log-log coordinates.*

A power law spectrum implies a linear relationship between the manifold harmonic coefficients and eigenvalue when plotted on a log scale. We assess the linearity of this relationship by computing the correlation coeffient, R between $\log\tilde{r}$ and $\log\lambda$. The results are given in Table 1. Negative values of R correspond to exponential decay, and all values computed are negative as expected. As a rule of thumb, R values in the range $[-1.0, -0.5]$ imply a strong linear relation in log-space, and therefore a strong power law relation between manifold harmonic coefficients and frequency. The mean correlation coefficient over all meshes was -0.888 with a variance of 0.0009. The average slope α for the meshes was -1.25 which corresponds closely with the findings of Graham and Field [GF07] who found that the best-fit slope over 137 photographs of natural scenes was -1.37

© 2010 The Author(s)
Journal compilation © 2010 The Eurographics Association and Blackwell Publishing Ltd.

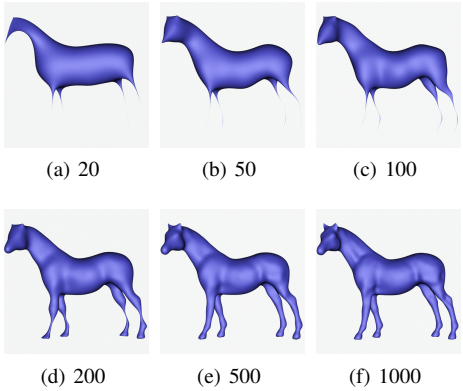

(a) 20 (b) 50 (c) 100

(d) 200 (e) 500 (f) 1000

Figure 5: *Horse reconstructed from varying numbers of manifold harmonic basis functions. Low frequency components describe the shape of the horse, and high frequency components represent detail.*

($R = -0.96$) and the best-fit slope over 124 paintings of natural scenes produced by artists was -1.23 ($R = -0.94$).

Qualitatively, the power-law behavior is is also apparent in Figure (5) which shows a mesh reconstructed from various numbers of basis functions. Using only the 20 lowest frequency basis functions the quadrupedal structure of the character becomes visually apparent, and much of the volume of the torso is filled. As the number of basis functions increases, progressively finer (smaller amplitude) details can be seen to emerge.

Some known allometric relations involve global geometric properties of the body, such as volume, surface area or length. Other relations are specific to anatomical regions. To accommodate both types of relations we present separate global and local allometric scaling techniques in the following sections. In both algorithms we presume that the input mesh is plausible, and generate new meshes which are also plausible.

3.1. Global allometric scaling

The global allometric scaling described in this section is determined by one parameter, and only biomechanical considerations are taken into account. Biewener [Bie90] reports that "mammalian skeletons experience peak locomotor stresses (force per area) that are 25 to 50% of their failure strength, indicating a safety factor of between two and four." This provides valuable information about how the biomechanics of terrestrial locomotion influence the size of the limbs. In particular it places bounds on the cross-sectional area of the limbs.

Furthermore, forces generated during motion are generally proportional to body weight, and the highest forces experienced are usually impact forces due to falling or jumping. These can be $5-10$ times body weight. By comparison, running may result in forces approximately $2-3$ times body weight [Ale85]. Rather than requiring the user to estimate safety factors, we assume that the safety factor in the scaled mesh will be equally to the safety factor in the original mesh. However, it would be trivial to incorporate variable safety factors, or activity levels into our system.

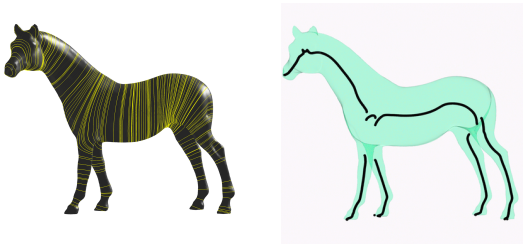

Figure 6: *Isocontours of the second manifold harmonic basis function (left) and mesh skeleton computed from centroids of isocontours (right). The isocontours provide us with a measure of local cross-sectional area, and the skeleton allows us to estimate bone lengths.*

Since shear stresses, τ, and compressive stresses, σ, are both given by F/A where F is the applied force and A is the cross-sectional area we can see that increased forces due to higher body weight can be mitigated by increased cross-sectional area. Bending stresses are more complicated since they depend on the cross-sectional shape (through the area moment of inertia). However, the stress can be reduced by decreasing the bending moment. This can be achieved by shortening the limb or decreasing the applied force. It can also be achieved by increasing the area moment of inertia, which we do not explicitly address.

By constraining the mesh deformation in terms of biomechanical stresses experienced during terrestrial locomotion we also constrain the range of valid input meshes. To apply our method to fish and other water-dwelling creatures bouyancy and stresses due to swimming should be considered. This reflects the connections between form and function which allometric laws embody. In particular, the differing relations between size and shape for aquatic animals as compared to terrestrial animals has been noted by many researchers. Thompson [Tho52] observed that the skeletons of large whales and smaller porpoises were remarkably similar due to the reduced effect of gravity on these creatures. Likewise, flying creatures will be constrained by additional internal stresses generated by lift forces. We do not foresee any problems incorporating these other biomechanical analyses into our system since they can be expressed in terms of geometrical quantities (length, volume, surface area, cross-sectional area) which we can estimate from the mesh. However, in this work, we restrict our analysis to quadrupedal animals.

© 2010 The Author(s)
Journal compilation © 2010 The Eurographics Association and Blackwell Publishing Ltd.

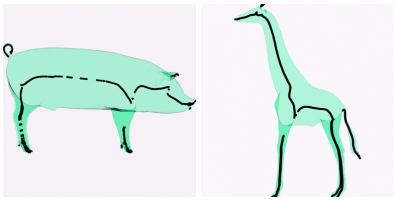

Figure 7: *Skeleton results for pig and giraffe.*

To estimate the body mass of a character we assume a constant material density, ρ, and then compute mass from the volume, $M = \rho V$. We use the method described by Mirtich [Mir05] for computing the volume of triangle meshes. Since our calculations are done in terms of ratios we do not require the user to input a value for ρ, and we can consider weight, mass, and volume to be equivalent.

To estimate cross-sectional area we again make use of the manifold harmonic decomposition. In particular we use the so-called Fiedler vector, the eigenvector/eigenfunction corresponding to the second smallest eigenvalue of the mesh Laplacian. The Fiedler vector and corresponding eigenvalue figure prominently in spectral graph partitioning and the study of graph topology. What makes it so useful for segmentation problems is that nearby vertices have similar values in the Fiedler vector. This implies that isocontours of the Fiedler vector should form short closed paths on the mesh. Critical points, where the isocontour length becomes zero, occur at mesh extremities. These properties make the area of the isocontours useful for characterizing peak stresses in the mesh. We rely on the user to manually select the isocontour which experiences peak stress. From the area of this contour and the volume of the mesh we can estimate the value of peak stress. From these contours we also compute the mesh skeleton which we make use of in the next section. The centroid of each contour is a point on the skeleton of the mesh. The isocontours of the Fiedler vector are shown in Figure (6) along with the computed skeleton. Additional skeleton results are shown in Figure (7). The skeleton we compute is a geometric medial axis rather than a true approximation of the anatomical skeleton. So, for example, our skeleton lacks features such as a skull and ribs. However, it is useful for approximating lengths.

The relationships between allometry, fractal systems and frequency domain power laws motivate the implementation of allometric scaling in terms of manifold harmonic coefficients. Consider the function

$$\tilde{x}_i'(\alpha, s) = s\tilde{x}_i\lambda_i^{\alpha}. \tag{4}$$

After applying this transformation to the coefficients they still obey a power law, but with a different exponent, so the underlying mesh still falls within the class of 'natural meshes'. The expected results of this function can be explained in terms of Figure (5). Note that the reconstruction

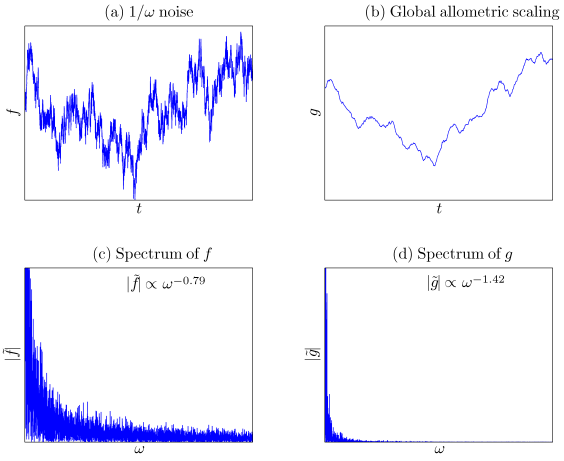

Figure 8: *Test of global allometric scaling in the DCT domain. A synthetic noise signal, f, and its spectrum, $|\tilde{f}|$, are shown on the left (a,c). Applying global allometric scaling as described in Equation (4) results in the signal g which has spectrum $\tilde{g}$ as shown on the right (b,d).*

using a few basis function reveals the skeletal shape and the torso. As higher frequencies are added the neck and then legs appear. High spatial frequencies correlate with small cross-sectional area. When $\alpha > 0$ the coefficients corresponding to small area shrink faster than those corresponding to high area. The expectation is that the limbs in these meshes will become thinner compared to the torso, for example. This corresponds to scale reduction in that the smaller creature can be supported by relatively thin legs. For $\alpha < 0$ the situation is reversed, and for $\alpha = 0$ the scaling is isometric.

Global allometric scaling was tested on synthetic one-dimensional signals with $1/f$ spectra. An example output of the experiment is shown in Figure 8. The power law exponent of the spectrum was computed by least-squares in log-space. After allometric scaling the exponent was recomputed. The example shown in Figure 8 was computed with $\alpha = 1.8$, and results in the power law exponent changing by a factor of 1.8 as expected.

Not all of the cross-sectional areas computed from isocontours are load-bearing, for example we do not expect the ears or tail of an animal to support the full body weight. With this in mind we manually select an isocontour with small cross-section in one of the limbs to characterize the peak stresses expected in the character. Then the peak stresses in the original mesh $\sigma_0 = M_0/A_0$. After scaling with isometric factor, s and allometric factor, α, we want the peak stresses to be equal, $\sigma_1(s,\alpha) = \sigma_0$. Since isometric scaling affects stress in a linear manner $\sigma_1(s,0) = \frac{s^3 V_0}{s^2 A_0} = s\sigma_0$, we can compute the isometric scale factor $s = \sigma_1(1,\alpha)/\sigma_0$ given α.

The global allometric scaling results in Figures (9) and

© 2010 The Author(s)
Journal compilation © 2010 The Eurographics Association and Blackwell Publishing Ltd.

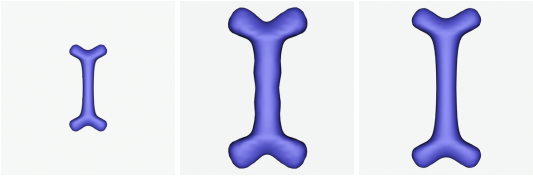

Figure 9: *Original bone (left), allometrically scaled bone (middle), isometrically scale bone (right). The proportions have changed in a way similar to the prediction of Galileo.*

Figure 10: *Original chair (middle), and allometrically scaled chair (left, right). Note that the scaling is effective when the topological genus is greater than 0.*

(10) demonstrate the nonuniform scaling we expect when trying to compensate for the square-cube law. The bone becomes proportionally thicker as it becomes larger, as predicted by Galileo in the sketch in Figure (2). The smaller chair can be supported by longer, thinner legs, and the larger chair has thicker, and proportionally shorter legs to support a higher weight. These results also demonstrate the generality of the scaling method with respect to topological genus.

3.2. Local allometric scaling

Local scaling requires a segmentation of the mesh which defines the anatomical regions. We developed a user-assisted technique based on the method presented by Zhang and Liu [LZ04]. An automatic oversegmentation of the mesh into 24 regions is first performed, then the user manually merges selected regions to obtain the 6 desired regions : head, neck, upper torso, lower torso, forelimbs and hindlimbs. From the segmentation we can obtain an indicator function for each region, I_{seg} such that $I_{seg}(x_i) = 1$ when vertex x_i is part of the specified region, and $I_{seg}(x_i) = 0$ otherwise. Then we define the vertex set $x_{seg} = I_{seg}x$.

The MHT of the segmented vertex set is performed in terms of basis functions, H, and lumped-mass matrix, D, of the original mesh

$$\tilde{x}_{seg} = x_{seg}DH. \tag{5}$$

Our approach to local allometric scaling is to perform power-law scaling on only the coefficients of basis functions which contribute most to the segmented vertex set. Since the basis functions are global it is not possible to guarantee

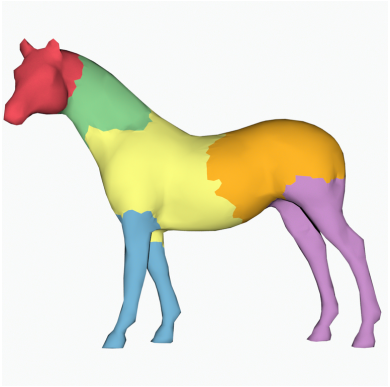

Figure 11: *Mesh segmentation used for local allometric scaling. The various regions will be allometrically scaled independently.*

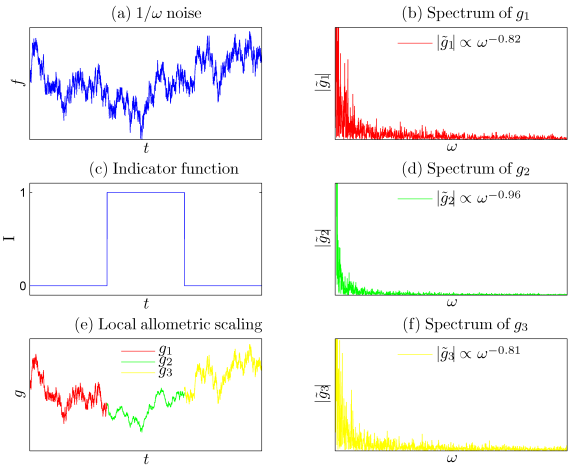

Figure 12: *Test of local allometric scaling in the DCT domain. Note that the region segmented by the indicator function (shown in green) can be locally scaled with only minor changes to the surronding regions.*

that this transformation will only change vertices in the segmented set, but we aim to minimize the distortions in other areas.

In formulating local allometric scaling we make use of the fact that if $|\tilde{x}|$ has power law form then $|\tilde{x}|^{1+\alpha}$ also has a power law form with similar exponent when α is small. The transformation of frequency coordinates is given by

$$\tilde{x}_i' = \mathrm{sgn}(\tilde{x}_i)|\tilde{x}_i|^{1+\alpha G(\tilde{x}_i, \tilde{x}_{seg,i})} \tag{6}$$

where G is the geometric mean defined as

$$G(a,b) = \begin{cases} \sqrt{ab} & \text{if } ab > 0 \\ 0 & \text{otherwise} \end{cases}. \tag{7}$$

© 2010 The Author(s)
Journal compilation © 2010 The Eurographics Association and Blackwell Publishing Ltd.

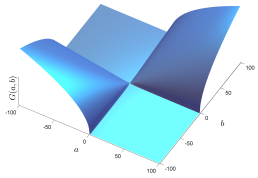

Figure 13: *The geometric mean, $G(a,b)$, of two variables, a and b.*

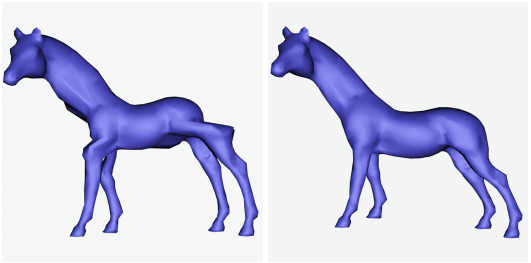

Figure 14: *Local allometric scaling of the torso of the horse mesh. Arithmetic manipulation of the spectrum results in discontinuities (left). Power-law manipulation of the spectrum gives a smoother result (right).*

The transformation in Equation (6) preserves the sign of the frequency coordinates, which prevents spurious reflections from occurring, and also avoids the generation of complex coordinates. The geometric mean of two numbers tends to be closer to the lower number, which makes it useful for isolating the coefficients which contribute most to the segmented region. When $\tilde{x}_i$ and $\tilde{x}_{seg,i}$ are both large, then the geometric mean will be large, but when either of the coefficients (or both coefficients) are small the geometric mean is small, as shown in Figure 13. The geometric mean of two numbers is always less than or equal to the arithmetic mean of two numbers. So when a coefficient contributes relatively little to the segmented region the exponent computed by Equation (6) will be close to one. When the coefficients are of opposite sign the geometric mean is 0 and no scaling is performed. Since coefficients of opposite sign contribute to geometric reflections in the reconstructed mesh we leave these coefficients unchanged to avoid large-scale mesh deformations.

Local allometric scaling was also tested on synthetic one-dimensional signals with $1/f$ spectra. An example output of the experiment is shown in Figure 12. An indicator function, I, was selected to simulate the effect of segmentation in one dimension. The spectrum of the segmented region $DCT(If)$ was computed.

The naive approach, arithmetically scaling the coefficients of the vertex set, has predictably bad results as shown in Figure (14). That is because this method is equivalent to simply scaling the segmented vertex set, which leads to discontinuities at the segmentation boundary. Our approach to local allometric scaling does not suffer from this consequence. Simply following arithmetic scaling with low-pass filter would also be unsatisfactory since some of the desired high frequency detail would be blurred as well.

Figure 15: *Local allometric scaling permits specific anatomical regions to be targeted for scaling. From left to right the torso shrinks, and from top to bottom the legs shorten. The original mesh is in the center.*

Local allometric scaling is a useful mesh editing tool by itself since it gives anatomical meaning to combinations of frequency coordinates for a mesh. We extend this idea even further by using allometric laws to connect relative rates of change of different regions to obtain biologically plausible results.

Results of local allometric scaling are shown in Figure (15). In this case local anatomical changes were made by explicitly specifying values of α_j in Equation (6). As expected, the scaling results in minor changes in pose and other non-local deformations, but no discontinuities are observed.

3.3. Biology-aware allometric scaling

Prothero [Pro92] tabulated allometric relations between different local variables for many species. The variables included length and diameter of forelimbs, hindlimbs and torso as a means of describing a simplified model composed of cylinders. We draw on this work, but segment the mesh further. We decompose the torso into chest and abdominal segments, and also add head and neck segments. Since the relations we present here are based on empirical measurements of quadupedal mammals, they may not give plausible results for other characters (such as humans, insects or fish). The optimization method we present can, however, be extended by incorporating relations which are appropriate for the species being modeled.

© 2010 The Author(s)
Journal compilation © 2010 The Eurographics Association and Blackwell Publishing Ltd.

Allometric relations between specific anatomical regions and mass can sometimes be explained theoretically in terms of physiology.

Biomechanical relations allow us to impose constraints which guarantee that the character has a musculoskeletal system which can resist internal stresses. Limb length is an important factor in theoretical analysis of locomotion [Ale03]. It is related to stride length and peak stress. Since stresses generated during locomotion are due to body forces, the connection to body mass is strong.

Cardiopulmonary relations are used to guarantee that the character has a cardiovascular system which can supply blood throughout the body, and a respiratory system capable of oxygenating the blood stream. Many cardiovascular parameters have allometric relations with body mass; including heart rate, blood pressure, stroke volume, length of aorta and heart mass [DL98]. Additionally, chest volume is proportional to both lung volume and heart volume. Furthermore heart volume is proportional to stroke volume which is an important variable in assessing the function of the circulatory system [Li96]. However, since girth measurements are easier to obtain and less prone to error, we use chest girth as a variable in the scaling algorithm. Since heart girth is proportional to chest girth, and chest girth is allometrically related to body mass, we can obtain a relation between chest girth and stroke volume.

Metabolic relations enforce the constraint that the character have a digestive system capable of generating enough energy for activity. The energy requirements dictate the mass of the digestive system which influences the size of the lower abdomen. The abdominal region contains organs vital to the digestive system, such as the stomach, liver, and intestines. Because of this function its size is influenced by metabolic parameters. The relation $M_{ab} \propto M_{body}^{0.74}$ [UJP98] is thought to be a direct consequence of Kleiber's law relating metabolic rate to body mass with an exponent of 0.75. This would imply that the volume of food in the gut is proportional to the energy metabolized.

Head and neck size. There is no general relation between head size and body mass which holds over a large number of species. For the families in which allometric relations have been observed the relation is negative, such as the relation in primates $M_{brain} \propto M_{body}^{0.78}$. Also, within a single species there is a negative allometry associated with maturation $M_{brain} \propto M_{body}^{0.70}$. We use the latter number in our experiments. The segment we have not addressed yet is the neck. Like the head, we find no general observations, except among creatures characterized by exceedingly long necks. Animals such as the giraffe and flamingo with very long necks must have high blood pressures in order to push blood up to the brain. We provide the user with a control for separately controlling this attribute using $1/3$ as the baseline value predicted by isometric scaling.

The anatomical measurements and the allometric relations we use in the biology-aware scaling algorithm are

$$\begin{aligned} \text{(foreleg length) } L_{fl} &\propto M_{body}^{0.360} \\ \text{(hindleg length) } L_{hl} &\propto M_{body}^{0.336} \\ \text{(chest girth) } G_{chest} &\propto M_{body}^{0.365} \\ \text{(head mass) } M_{head} &\propto M_{body}^{0.700} \\ \text{(abdominal mass) } M_{ab} &\propto M_{body}^{0.740} \end{aligned} \tag{8}$$

however, the selection of mass, length or girth measurements, and the values of the exponents can be freely selected by the user to achieve desired results. We estimate lengths of regions from the skeleton and the segmentation. The diameter (the length of the longest geodesic path between vertices) of the skeleton is taken to be the length. Region volumes are estimated by segmenting the mesh, capping the open boundaries, and computing the volume of each submesh. Girth measurements are computed by calculating the length of isocontours of the Fiedler vector.

We perform scaling which takes all of the above relations into account using the following extension of Equation (6)

$$\tilde{x}_i'(\alpha, s) = s\,\mathrm{sgn}(\tilde{x}_i)|\tilde{x}_i|^{1+\alpha_0+\sum_{j=1}^{6}\alpha_j G(\tilde{x}_i,\tilde{x}_{j,i})}, \tag{9}$$

where α_0 is the global allometric scale, and j indexes the 6 segmented regions. As in the global scaling case, we compute the isometric scale factor, s, which will make the mesh biomechanically plausible.

We use an energy minimization approach to perform local allometric scaling subject to the constraints in Equation (8). To limit the amount of mesh deformation performed, we set a target mass $M_{body,1} = 1.1 M_{body,0}$ when scaling up, and $M_{body,1} = 0.9 M_{body,0}$ when scaling down, where $M_{body,0}$ is the initial volume of the mesh. Given this target mass, we can set target values for the variables on the left-hand side of Equation (8),

$$\begin{aligned} L_{fl,1} &= r^{0.360} L_{fl,0} \\ L_{hl,1} &= r^{0.336} L_{hl,0} \\ G_{chest,1} &= r^{0.365} G_{chest,0} \\ M_{head,1} &= r^{0.700} M_{head,0} \\ M_{ab,1} &= r^{0.740} M_{ab,0} \end{aligned} \tag{10}$$

where r is the ratio of target mass to initial mass $M_{body,1}/M_{body,0}$, which is 1.1 or 0.9 in our experiments. Larger or smaller mass ratios can be achieved by repeated applications of the optimization procedure with recomputation of the MHB and MHT between iterations. The energy we seek to minimize is given by

$$\begin{aligned} E(\tilde{x}') = {} & (M_{body}(\tilde{x}') - M_{body,1})^2 + (L_{fl}(\tilde{x}') - L_{fl,1})^2 + \ldots \\ & (L_{hl}(\tilde{x}') - L_{hl,1})^2 + (G_{chest}(\tilde{x}') - G_{chest,1})^2 + \ldots \\ & (M_{head}(\tilde{x}') - M_{head,1})^2 + (M_{ab}(\tilde{x}') - M_{ab,1})^2 + \ldots \\ & (\sigma(\tilde{x}') - \sigma_1)^2 \end{aligned} \tag{11}$$

© 2010 The Author(s)
Journal compilation © 2010 The Eurographics Association and Blackwell Publishing Ltd.

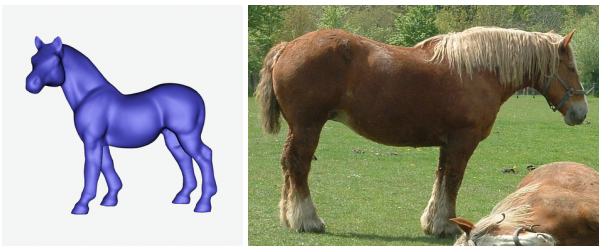

(a) Breton

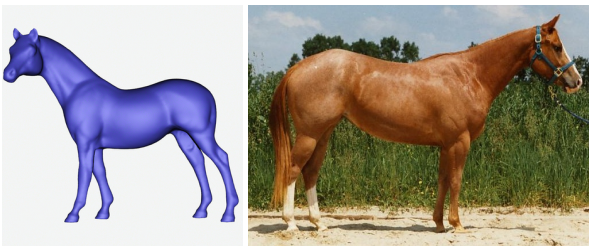

(b) Quarterhorse (original mesh)

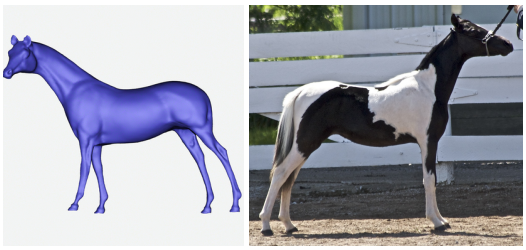

(c) Miniature stallion

Figure 16: *Visual comparison of global allometric scaling results (left) and photographs of horse breeds (right).*

where σ is the biomechanical stress described in Section 3.1.

We find the values of $s, \{\alpha\}$ which minimize Equation (11) using a nonlinear least-squares solver [NW00] based on the trust-region Newton-CG method.

4. Results

We processed 12 triangle meshes representing quadrupedal terrestrial animals. The meshes were preprocessed to remove unreferenced vertices and non-manifold faces, then simplified to contain fewer than 100,000 vertices. The simplification process reduces the memory requirements for storing the MHB which may not fit into main memory for large meshes. The MHB and MHT of each mesh were computed, then a skeleton was automatically extracted and a user-assisted segmentation was produced. The data were processed on desktop computer with Intel Quad Core QX6700 2.66 GHz CPU and 4 GB RAM.

Global allometric scaling applied to the horse mesh is shown in Figure (16) along with images of actual horse breeds for reference. Horse breeds vary over a wide range of scales, which leads to much variation in shape. Since there are many feasible horse shapes we do not expect an exact match, but there are many similarities between the meshes and the photographs. The Breton is a large draft horse characterized by stocky, powerful legs, a short neck, and a wide chest. The corresponding mesh has matching characteristics, however the length of the torso of the actual horse is longer. The miniature stallion in the reference photo has spindly legs, a narrow torso and a long thin neck, much like the corresponding mesh.

Additional results for global allometric scaling are shown in Figure (17) for camel, pig, elephant, cow and giraffe meshes. The anatomical features scale in the same way as the horse mesh - the enlarged creatures tend to have shorter and thicker body parts and the shrunken meshes are longer and thinner. When performing large deformations, as in Figure (19), the transformed spectrum of the input mesh may not correspond to the spectrum of resulting mesh. This is because the new mesh does not necessarily have the same manifold harmonic basis as the input mesh. For this reason, we perform large scale changes iteratively - applying a small scale change, recomputing the MHB and repeating, as in the biology-aware allometric scaling shown in Figure (18)

The allometric scaling process we have described does not perform any collision detection, and so some self-intersections may be generated. This can be seen in the tail of the cow in Figure (17). Another visible artifact is high frequency rippling, as seen in Figures (9,10), and smoothing of some fine details. The smoothing effect is most noticable in allometric minification since this process causes high frequency details to be attenuated faster than low frequency details. Some sharp corners and points degenerate into line-like features, such as the tail of the elephant, and the horns of the cow. These issues have been mitigated in the character mesh results by a combination of low-pass filtering of the input to the scaling algorithm, and detail enhancement of the output [VL08].

5. Conclusions and Future Work

We have presented a novel character editing technique which respects biological and physiological principles. The resulting meshes are plausible in terms of biomechanical constraints and important biological processes which impact scale. In this work we consider the impact of the cardiovascular and metabolic systems. Our technique does not perform any time-consuming numerical simulation of biological processes. Instead, it relies on previously observed allometric relations between scale and function. We do not require the user to input values for any physical or biological parameters, but the input mesh is assumed to be plausible. Users interface with the allometric relations in a strictly qualitative way - simply choosing to increase or decrease mass. We have demonstrated that the methods we present

© 2010 The Author(s)
Journal compilation © 2010 The Eurographics Association and Blackwell Publishing Ltd.

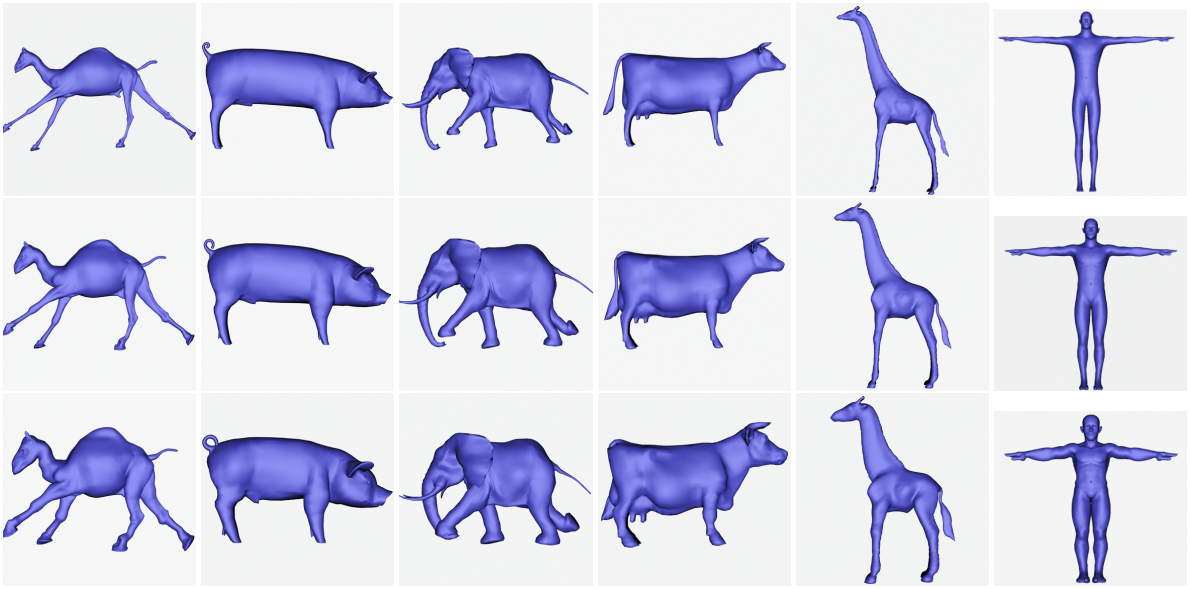

Figure 17: *Global allometric scaling results. Allometric minification with* $\alpha = -0.1$ *(top), the input mesh (middle) and allometric magnification with* $\alpha = +0.1$ *(bottom) for several meshes. The overall scale of each mesh has been normalized in this figure.*

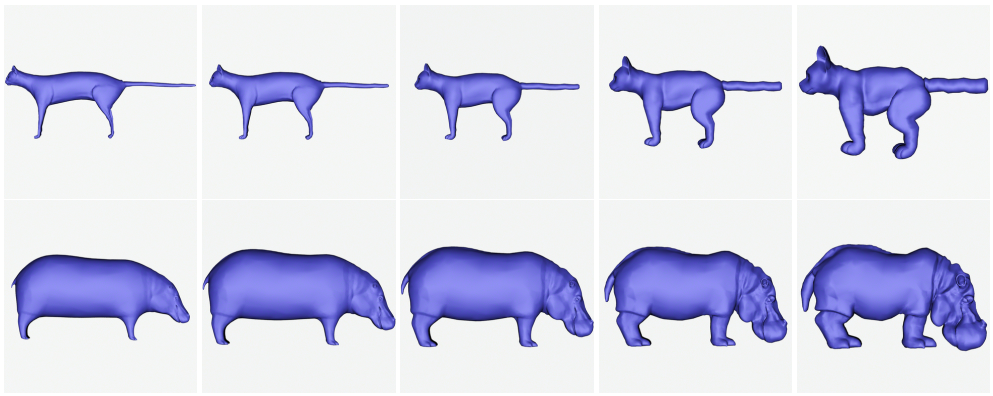

Figure 18: *Biology-aware allometric scaling results. Relative scales of anatomical regions have been linked to make the scaling match observed allometric relations which are governed by biological function. The original meshes are in the middle column. The overall scale of each mesh has been normalized in this figure.*

© 2010 The Author(s)
Journal compilation © 2010 The Eurographics Association and Blackwell Publishing Ltd.

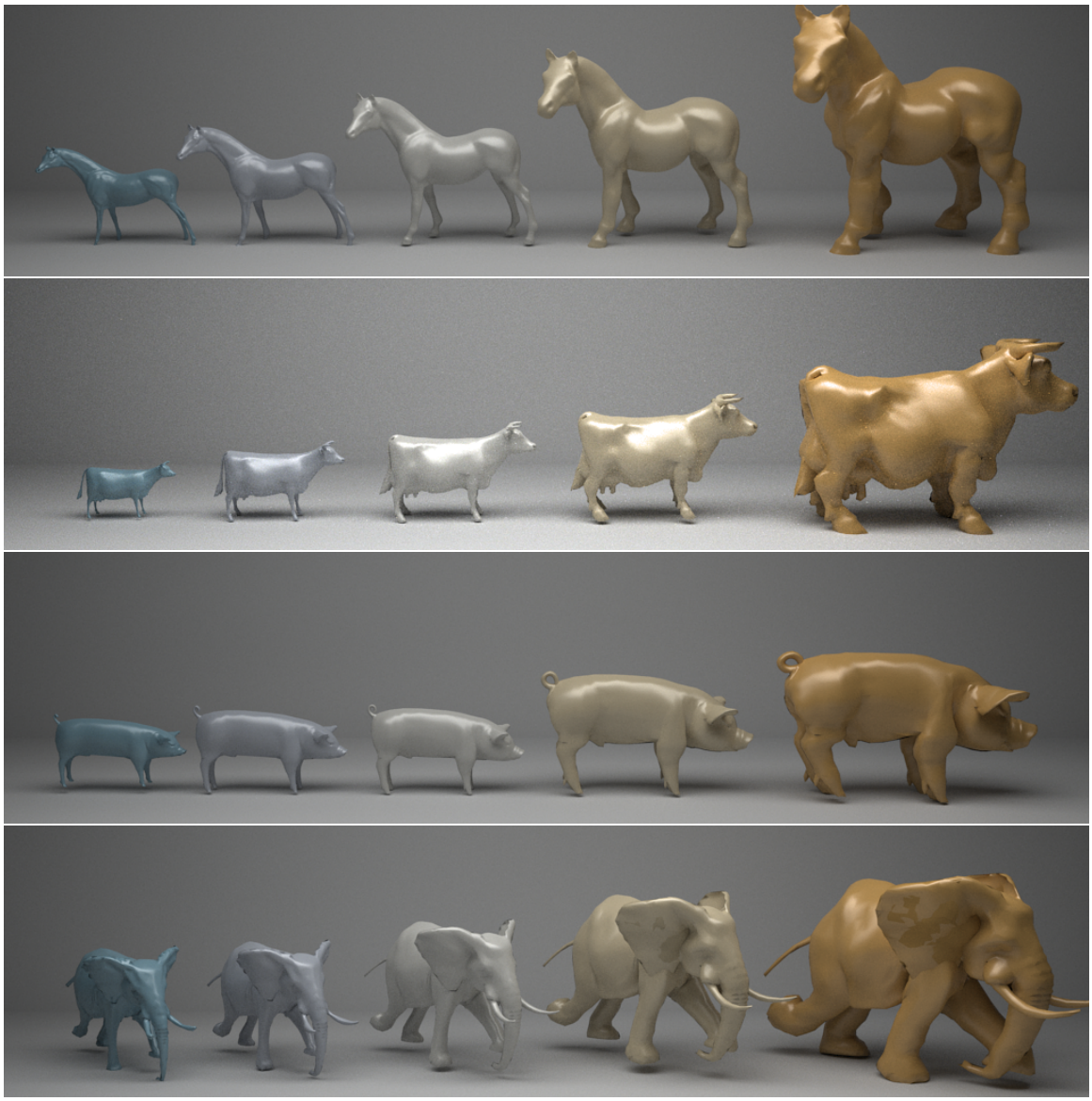

Figure 19: *Allometric scaling of horse, cow, elephant and pig meshes. The original mesh is in the middle, and it has been scaled larger (to right) and smaller (to left) such that biomechanical constraints are satisfied.*

© 2010 The Author(s)
Journal compilation © 2010 The Eurographics Association and Blackwell Publishing Ltd.

give reasonable results by providing visual comparison with known horse breeds.

In future work we plan to implement additional rules and make a clearer distinction between interspecies and intraspecies allometry. Intraspecies allometric laws govern the development of animals of the same species as they mature, while interspecies laws govern differences among adults of different species. The user will then be able to pick a set of rules based on the biological class (e.g. mammal, reptile, insect) best matching the mesh, and optionally include effects due to age. Additional biomechanical relations will be incorporated to account for other forms of locomotion, such as swimming and flying. This will permit the system to be extended from quadrupeds to fish, birds and other species. We also plan to further explore the application of the Fiedler vector to skeleton generation for character animation.

There are other geometrical constraints to consider when scaling biological structures, including surface area-volume relations which govern how heat due to metabolism is dissipated. This typically becomes an issue at very small scales, such as with rodents and insects.

Acknowledgements

Meshes were obtained from Princeton database described in *A Benchmark for 3D Mesh Segmentation*, the Princeton *Suggestive Contour Gallery* the Stanford *3D scanning repository* and the Georgia Tech *Large Geometric Models Archive*. Photo credits : Jean (Figure 16a), Rumo (Figure 16b), and Eponimm (Figure 16c). Photos used under Creative Commons license.

References

[ACP03] ALLEN B., CURLESS B., POPOVIĆ Z.: The space of human body shapes: reconstruction and parameterization from range scans. *ACM Transactions on Graphics (TOG) 22*, 3 (2003), 587–594. 4

[Ale85] ALEXANDER R.: The maximum forces exerted by animals. *The Journal of experimental biology 115* (1985), 231. 6

[Ale03] ALEXANDER R.: *Principles of animal locomotion*. Princeton Univ Press, 2003. 10

[ASK*05] ANGUELOV D., SRINIVASAN P., KOLLER D., THRUN S., RODGERS J., DAVIS J.: Scape: shape completion and animation of people. *ACM Transactions on Graphics (TOG) 24*, 3 (2005), 408–416. 4

[BCG05] BEN-CHEN M., GOTSMAN C.: On the optimality of spectral compression of mesh data. *ACM Trans. on Graphics 24*, 1 (2005), 60–80. 4

[Bie90] BIEWENER A.: Biomechanics of mammalian terrestrial locomotion. *Science 250*, 4984 (1990), 1097. 6

[Bon69] BONNER J.: *The scale of nature*. Harper and Row, 1969. 1

[Bon06] BONNER J.: *Why size matters: from bacteria to blue whales*. Princeton Univ Press, 2006. 1

[Bri08] BRIDSON R.: *Fluid simulation for computer graphics*. AK Peters Ltd, 2008. 3

[DBG*06] DONG S., BREMER P.-T., GARLAND M., PASCUCCI V., HART J. C.: Spectral surface quadrangulation. In *SIGGRAPH* (2006), pp. 1057–1066. 4

[dGGV08] DE GOES F., GOLDENSTEIN S., VELHO L.: A hierarchical segmentation of articulated bodies. *Computer Graphics Forum (Symposium on Geometry Processing) 27*, 5 (2008), 1349–1356. 4

[DL98] DRZEWIECKI G., LI J.: *Analysis and assessment of cardiovascular function*. Springer, 1998. 10

[DRW01] DODDS P., ROTHMAN D., WEITZ J.: Re-examination of the" 3/4-law" of metabolism. *Journal of theoretical biology 209*, 1 (2001), 9. 3

[Ebe03] EBERT D.: *Texturing & Modeling: A Procedural Approach*. Morgan Kaufmann, 2003. 3

[FFL*96] FALCO T., FRANCIS F., LOVEJOY S., SCHERTZER D., KERMAN B., DRINKWATER M.: Universal multifractal scaling of synthetic aperture radar images of sea-ice. *IEEE Transactions on Geoscience and Remote Sensing 34*, 4 (1996), 906–914. 3

[GCFdS54] GALILEI G., CREW H., FAVARO A., DE SALVIO A.: *Dialogues concerning two new sciences*. Dover Publications, 1954. 1, 2

[GF07] GRAHAM D., FIELD D.: Statistical regularities of art images and natural scenes: Spectra, sparseness and nonlinearities. *Spatial Vision 21*, 1-2 (2007), 149–164. 5

[GGS03] GOTSMAN C., GU X., SHEFFER A.: Fundamentals of spherical parameterization for 3d meshes. *ACM Trans. on Graphics 22*, 3 (2003), 358–363. 4

[Gou66] GOULD S.: Allometry and size in ontogeny and phylogeny. *Biol. Rev 41*, 4 (1966), 587–640. 3

[Hal28] HALDANE J.: On being the right size. *A treasury of science* (1928), 321–325. 1, 2

[Hux32] HUXLEY J.: *Problems of relative growth*. L. MacVeagh, The Dial Press, 1932. 2

[IYKI08] IJIRI T., YOKOO M., KAWABATA S., IGARASHI T.: Surface-based growth simulation for opening flowers. In *GI '08: Proceedings of graphics interface 2008* (2008), pp. 227–234. 3

[JZ07] JAIN V., ZHANG H.: A spectral approach to shape-based retrieval of articulated 3d models. *Computer Aided Design 39* (2007), 398–407. 4

[KLT05] KATZ S., LEIFMAN G., TAL A.: Mesh segmentation using feature point and core extraction. *The Visual Computer (Special Issue of Pacific Graphics) 21*, 8-10 (2005), 649–658. 4

[KSO04] KOLLURI R., SHEWCHUK J. R., O'BRIEN J. F.: Spectral surface reconstruction from noisy point clouds. In *Proc. Eurographics Symp. on Geometry Processing* (2004), pp. 11–21. 4

[LDC93] LAM N., DE COLA L.: *Fractals in geography*. PTR Prentice Hall, 1993. 3

[LH05] LEORDEANU M., HEBERT M.: A spectral technique for correspondence problems using pairwise constraints. In *Proc. Int. Conf. on Comp. Vis.* (October 2005), vol. 2, pp. 1482–1489. 4

[Li96] LI J.: *Comparative cardiovascular dynamics of mammals*. CRC, 1996. 3, 10

[LST09] LEE S., SIFAKIS E., TERZOPOULOS D.: Comprehensive biomechanical modeling and simulation of the upper body. *ACM Transactions on Graphics (TOG) 28*, 4 (2009), 99. 3

[LZ04] LIU R., ZHANG H.: Segmentation of 3d meshes through spectral clustering. In *Proc. of Pacific Graphics* (2004), pp. 298–305. 4, 8

© 2010 The Author(s)
Journal compilation © 2010 The Eurographics Association and Blackwell Publishing Ltd.

[Man79] MANDELBROT B.: Fractals: form, chance and dimension. 3

[MCBH07] MATEUS D., CUZZOLIN F., BOYER E., HORAUD R.: Articulated shape matching by robust alignment of embedded representations. In *ICCV '07 Workshop on 3D Representation for Recognition* (2007). 4

[Mir05] MIRTICH B.: Fast and accurate computation of polyhedral mass properties. *Graphics Tools: The JGT Editors' Choice* (2005). 7

[MTAD08] MULLAN P., TONG Y., ALLIEZ P., DESBRUN M.: Spectral conformal parameterization. *Computer Graphics Forum (Symposium on Geometry Processing) 27*, 5 (2008), 1487–1494. 4

[MVN68] MANDELBROT B., VAN NESS J.: Fractional Brownian motions, fractional noises and applications. *SIAM review 10*, 4 (1968), 422–437. 3

[NW00] NOCEDAL J., WRIGHT S.: *Numerical optimization*. Springer, 2000. 11

[OSG08] OVSJANIKOV M., SUN J., GUIBAS L.: Global intrinsic symmetries of shapes. *Computer Graphics Forum (Symposium on Geometry Processing) 27*, 5 (2008), 1341–1348. 4

[Per85] PERLIN K.: An image synthesizer. *SIGGRAPH Comput. Graph. 19*, 3 (1985), 287–296. 3

[PHL*09] PALUBICKI W., HOREL K., LONGAY S., RUNIONS A., LANE B., MECH R., PRUSINKIEWICZ P.: Self-organizing tree models for image synthesis. *ACM Transactions on Graphics 28*, 3 (2009), 58:1–10. 4

[PL90] PRUSINKIEWICZ P., LINDENMAYER A.: *The algorithmic beauty of plants*. Springer-Verlag New York, Inc., 1990. 4

[Pro92] PROTHERO J.: Scaling of bodily proportions in adult terrestrial mammals. *American Journal of Physiology- Regulatory, Integrative and Comparative Physiology 262*, 3 (1992), 492. 9

[Pru86] PRUSINKIEWICZ P.: Graphical applications of L-systems. In *Proceedings of Graphics Interface '86 / Vision Interface '86* (1986), pp. 247–253. 4

[RCG08] RONG G., CAO Y., GUO X.: Spectral mesh deformation. *The Visual Computer 24*, 7 (2008), 787–796. 5

[Rey88] REYNOLDS, C. W.: Flocks, Herds, and Schools: A Distributed Behavior Model. *Computer Graphics 21*, 4 (1988), 25–34. 3

[RSAT04] REINHARD E., SHIRLEY P., ASHIKHMIN M., TROSCIANKO T.: Second order image statistics in computer graphics. In *Proceedings of the 1st Symposium on Applied perception in graphics and visualization* (2004), ACM New York, NY, USA, pp. 99–106. 3, 5

[SF93] STAM J., FIUME E.: Turbulent wind fields for gaseous phenomena. In *Proceedings of the 20th annual conference on Computer graphics and interactive techniques* (1993), ACM New York, NY, USA, pp. 369–376. 3

[SL87] SCHERTZER D., LOVEJOY S.: Physical modeling and analysis of rain and clouds by anisotropic scaling multiplicative processes. *J. Geophys. Res 92*, D8 (1987), 9693–9714. 3

[Ter99] TERZOPOULOS D.: Artificial life for computer graphics. *Communications of the ACM 42*, 8 (1999), 42. 3

[Ter08] TERZOPOULOS D.: Autonomous virtual humans and lower animals: from biomechanics to intelligence. In *AAMAS '08: Proceedings of the 7th international joint conference on Autonomous agents and multiagent systems* (2008), pp. 17–20. 3

[Tho52] THOMPSON D.: *On Growth and Form*. Cambridge University Press, 1952. 1, 6

[Tor98] TORRANCE R.: Allometric algorithms and the work of the heart. *Respiration physiology 113*, 1 (1998), 95–99. 3

[Tu99] TU X.: *Artificial animals for computer animation: biomechanics, locomotion, perception, and behavior*. Springer Verlag, 1999. 3

[Tur52] TURING A. M.: The chemical basis of morphogenesis. *Philosophical Transactions of the Royal Society (B) 237* (1952), 37–72. 3

[Tur91] TURK G.: Generating textures on arbitrary surfaces using reaction-diffusion. In *Proceedings of the 18th annual conference on Computer graphics and interactive techniques* (1991), pp. 289–298. 3

[TW90] TERZOPOULOS D., WATERS K.: Physically-based facial modeling, analysis, and animation. *Journal of visualization and Computer Animation 1*, 2 (1990), 73–80. 3

[UJP98] ULIJASZEK S., JOHNSTON F., PREECE M.: *The Cambridge encyclopedia of human growth and development*. Cambridge Univ Press, 1998. 10

[VL08] VALLET B., LÉVY B.: Spectral geometry processing with manifold harmonics. *Computer Graphics Forum (Eurographics) 27*, 2 (2008), 251–260. 4, 5, 11

[WBE97] WEST G., BROWN J., ENQUIST B.: A general model for the origin of allometric scaling laws in biology. *Science 276*, 5309 (1997), 122. 3

[WK91] WITKIN A., KASS M.: Reaction-diffusion textures. In *Proceedings of the 18th annual conference on Computer graphics and interactive techniques* (1991), pp. 299–308. 3

[ZB04] ZHANG H., BLOK H. C.: Optimal mesh signal transforms. In *Proc. of Geometric Modeling and Processing* (2004), pp. 373–379. 4

[Zha04] ZHANG H.: Discrete combinatorial laplacian operators for digital geometry processing. In *Proc. SIAM Conf. on Geom. Design and Comp.* (2004), pp. 575–592. 4

[ZKK02] ZIGELMAN G., KIMMEL R., KIRYATI N.: Texture mapping using surface flattening via multidimensional scaling. *IEEE Trans. Vis. & Comp. Graphics 8*, 2 (2002), 198–207. 4

[ZL05] ZHANG H., LIU R.: Mesh segmentation via recursive and visually salient spectral cuts. In *Proc. of Vision, Modeling, and Visualization* (2005). 4

[ZSGS04] ZHOU K., SNYDER J., GUO B., SHUM H.-Y.: Isocharts: Stretch-driven mesh parameterization using spectral analysis. In *Proc. Eurographics Symp. on Geometry Processing* (2004). 4

[ZvKD07] ZHANG H., VAN KAICK O., DYER R.: Spectral mesh processing. *(revised and extended version of Eurographics 2007 STAR report), Computer Graphics Forum* (2007). 4

© 2010 The Author(s)
Journal compilation © 2010 The Eurographics Association and Blackwell Publishing Ltd.